Carnegie Observatories Astrophysics Series, Vol. 3:
Clusters of Galaxies: Probes of Cosmological Structure and Galaxy Evolution, 2004
ed. J. S. Mulchaey, A. Dressler, and A. Oemler (Pasadena; Carnegie Observatories:
http://www.ociw.edu/ociw/symposia/series/symposium3/proceedings.html)

Hα-derived Star Formation Rates of $0.6 < z < 0.8$ Galaxy Clusters

R. A. FINN and D. ZARITSKY
University of Arizona

Abstract

We present Hα-derived star-formation rates for the $z = 0.845$ galaxy cluster CL J0023+0423B and demonstrate that near-infrared, narrow-band Hα imaging is a powerful way to sample the entire star-forming and post-starburst galaxy population in distant clusters. Comparison with spectroscopy shows that the number of false detections is low, and our Hα equivalent widths show reasonable correlation with spectroscopically determined [O II] equivalent widths. We compare the number of star-forming galaxies detected in our narrow-band images with the number found by a previously published spectroscopic survey and estimate that the spectroscopic survey is missing over 60% of star-forming galaxies in this cluster. Results on our entire sample of seven $z \approx 0.8$ clusters will be published in the near future, and we will be able to form a more comprehensive picture of the star-formation properties of $z \approx 0.8$ galaxy clusters.

1.1 Introduction

Galaxy populations in local clusters contain a higher fraction of early-type galaxies and older average stellar populations than field galaxies. While higher redshift clusters contain a higher fraction of blue, star-forming galaxies - the Butcher-Oemler effect (Butcher & Oemler, 1984), current studies indicate that the star-formation rates in high-redshift clusters are still depressed relative to coeval field galaxies (e.g. Balogh et al., 1997, 1998; Postman et al., 2001). By measuring the amount and radial dependence of star-formation rates for a sample of seven $z \simeq 0.8$ clusters, we investigate the physical processes behind the Butcher-Oemler effect. We derive star-formation rates from Hα emission using narrow-band near-infrared imaging. We use these data in conjunction with existing broad-band imaging and spectroscopy to link star-formation rates to the global properties of galaxies. We are making two significant strides in this program. First, we are creating a star-formation limited sample, not a magnitude-limited sample. Second, we are measuring star-formation rates from the Hα line, which is more directly related to star formation and less affected by dust and metallicity than the more commonly used [O II] line. Our star-formation limited sample allows us to determine the integrated star formation of a cluster.

Our sample consists of four $z \approx 0.8$ clusters from the Las Campanas Distant Cluster Survey (LCDCS, Zaritsky et al., 1997), and three additional clusters selected from the literature. The LCDCS clusters are part of a larger sample of ten $z \approx 0.5$ and ten $z \approx 0.8$ LCDCS clusters being studied by the EDisCS group. In this paper we present preliminary results on CL J0023+0423B, one of the clusters selected from the literature.

We choose CL J0023+0423B as part of our cluster sample because its redshifted Hα emission lies in a standard near-infrared narrow-band filter and because it has been studied extensively using *HST* WFPC2 imaging and Keck imaging and spectroscopy (Postman et al., 1998; Lubin et al., 1998). Postman et al. (1998) measure a velocity dispersion of 400 km/s from seventeen $\bar{z} = 0.845$ galaxies and from this determine a cluster mass of $\sim 3-6 \times 10^{14}\ h^{-1}\ \mathrm{M}_{\odot}$. The velocity distribution differs significantly from Gaussian, which implies that the cluster is not virialized, and no X-ray detections exist to date.

CL J0023+0423B also distinguishes itself from more massive clusters in terms of its morphological mix. Lubin et al. (1998) use WFPC2 imaging to visually classify the morphology of galaxies and find an early-type fraction of $\leq 33\%$, which is comparable to that of the field. Spectra of two galaxies that Lubin et al. (1998) classify as E/S0 galaxies show signs of recent star formation. The Hα imaging presented below paints a more detailed picture of the star-formation properties of the cluster galaxies, and we investigate the star-formation properties of the two E/S0 galaxies in more detail.

1.2 Observations and Data Reduction

For each cluster, we obtain narrow (1-2%) and J-band images using the PISCES near-infrared camera (McCarthy et al., 2001) at the 6.5m MMT. Images are reduced using standard near-infrared data reduction procedures (see McCarthy et al., 2001). We use SExtractor (Bertin & Arnouts, 1996) for source photometry. The J-band flux, scaled by the ratio of narrow-to-J filter throughputs, is used for continuum subtraction. For CL J0023+0423B, 3 σ flux limits correspond to 0.2 $h^{-2}\ \mathrm{M}_{\odot}\ \mathrm{yr}^{-1}$ and the minimum reliable equivalent width is 10 Å. Hα flux is converted to star-formation rate using the Kennicutt relation (Kennicutt, 1998).

1.3 Results

The distribution of star-formation rates is shown in the left panel of Figure 1.1. We detect 32 galaxies with $> 3\ \sigma$ emission and equivalent widths > 10 Å. The integrated star-formation rate for these $> 3\ \sigma$ emission sources is 30.2 $h^{-2}\ \mathrm{M}_{\odot}\ \mathrm{yr}^{-1}$ with an average star-formation rate of 0.9 $h^{-2}\ \mathrm{M}_{\odot}\ \mathrm{yr}^{-1}$. In the right panel of Figure 1.1 we plot the continuum-subtracted flux versus projected radial distance from the cluster center for all galaxies. The cluster is not centrally concentrated, so the cluster center is not well-determined. We use the dynamical center determined by Postman et al. (1998). We see elevated star-formation rates for radii $>$100 h^{-1} kpc projected distance and observe no trend in star-formation rates with radius. This cluster is not very massive so comparison with low-redshift massive clusters is difficult. Our areal coverage is complete to 300 h^{-1} kpc and cuts off entirely at 500 h^{-1} kpc. The limited field size and uncertainty in the position of the cluster center preclude further analysis on the radial dependence of star-formation rates for this cluster.

1.3.1 Cross-Check with Spectroscopy

Postman et al. (1998) have published spectroscopy for 127 objects in the LRIS field of CL J0023+0423B.Seventeen are confirmed cluster members at $z = 0.845$, and another seven are associated with a group at $z = 0.827$. We have matched 32 spectroscopic targets with galaxies in our J-band image. The redshift information provides a valuable check on

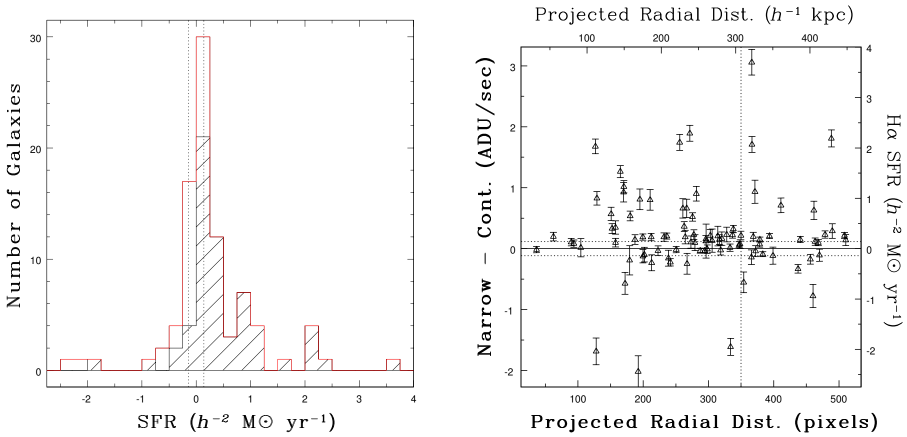

Fig. 1.1. (Left) Distribution of Hα-derived star-formation rates for all galaxies in CL J0023+0423B field (solid line) and galaxies with equivalent width >10 Å (shaded histogram). Vertical dotted lines marked 3 σ flux limits. Negative star-formation rates indicate objects with significant Hα absorption. (Right) Continuum-subtracted narrow-band flux versus projected radial distance from cluster center for all galaxies. Horizontal dotted lines show 3 σ flux limits. Vertical dotted line marks radius beyond which areal coverage is incomplete.

the validity of our Hα equivalent width measurements. We find one significant detection from a non-cluster member at $z = 0.922$. This detection can not be attributed to emission or absorption from another spectral feature. From comparison with the spectroscopic sample of Postman et al. (1998), we conclude that contamination from non-cluster members is small (1/32).

1.3.2 Completeness of Spectroscopic Surveys

How much star formation is missed in spectroscopic surveys? To answer this, we plot the distribution of equivalent widths measured from our Hα imaging and compare this to Hα equivalent widths of the seventeen cluster members detected by Postman et al. (1998) in the left panel of Figure 1.2. We multiply the Postman et al. (1998) [O II] equivalent widths by 2.5 to approximate the Hα equivalent width (Kennicutt, 1992a,b). The spectroscopy covers a larger area on the sky than our narrow-band imaging, but here we compare only the total number of star-forming galaxies detected with each method. We apply a minimum equivalent width cut of 10 Å to separate star-forming galaxies. We detect 32 galaxies with both an equivalent width >10 Å and Hα flux >3 σ, and Postman et al. detect 12. A few of our detections may be non-cluster galaxies, so we therefore estimate that the Postman et al. (1998) spectroscopic survey misses ∼60% of the star-forming galaxies in this cluster.

1.3.3 Morphological Dependence of Star-formation Rates

Lubin et al. (1998) use WFPC2 imaging to visually classify the 200 brightest galaxies in the CL J0023+0423B field. We use these visual morphological classifications to relate narrow-band equivalent width to galaxy morphology. In Figure 1.2, we plot the narrow-band equivalent width versus galaxy T-type for 39 galaxies that are either confirmed cluster

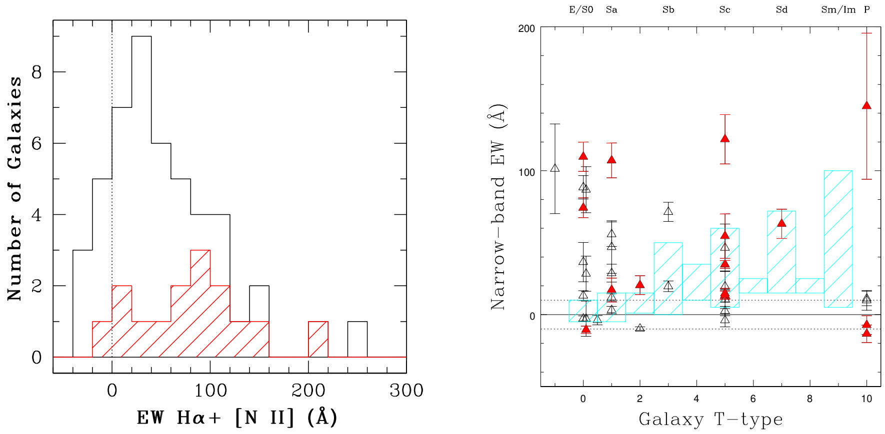

Fig. 1.2. (Left) Histogram of Hα + [NII] equivalent widths from this study (solid-line histogram) with those from the Postman et al. (1998) spectroscopic survey (shaded histogram). We detect 32 galaxies with equivalent width >10 Å, and Postman et al. (1998) detect 12. (Right) Narrow-band equivalent width versus galaxy T-type (Lubin et al. 1998a) for confirmed and possible cluster members. Galaxies with some sign of interaction are shown with solid red triangles. Shaded areas show range of equivalent widths for sample of nearby galaxies (Kennicutt 1998).

members or galaxies with undetermined redshifts (possible cluster members). We denote our equivalent width detection thresholds with horizontal dotted lines. The shaded boxes show the range of observed equivalent widths for a sample of nearby galaxies (Kennicutt, 1998). We observe significant equivalent widths in several E/S0 galaxies, and this is strikingly different from the Kennicutt (1998) results. However, we use GALFIT (Peng et al., 2002) to model the galaxy profiles of two spectroscopically confirmed cluster members that Lubin et al. (1998) classify as elliptical and which show active star formation. We find that they are best fit with exponential disk profiles. Lubin et al. (1998) also say that these galaxies have blue colors and spectral properties indicative of ongoing star formation. Therefore, their visual classification as early-type is tentative. We will reanalyze all galaxy profiles in the WFPC2 image using GALFIT to see if any ellipticals show signs of current of recent star formation.

1.3.4 Comparison of [O II] and Hα-derived Star-formation Rates

Eight spectroscopically confirmed cluster galaxies lie on our Hα image, and we compare the Postman et al. (1998) [O II] equivalent widths to our Hα equivalent widths in the left panel of Figure 1.3. The solid lines shows the empirical relation for local galaxies (Kennicutt, 1992a,b). We calculate [O II] star-formation rates from [O II] equivalent widths using Equation 2 from Postman et al. (2001). We plot the resulting [O II]-derived star-formation rates versus Hα-derived star-formation rates in the right panel of Figure 1.3. The red arrow shows redenning vector for 1 magnitude of extinction at Hα. This is the relevant redenning for [O II] as well because the [O II] star-formation rate is calibrated from Hα (Kennicutt, 1998). The sample is small and we have simplified our calculation of the [O II] star-formation rate. With these caveats in mind, we note that [O II] seems to underestimate the Hα-derived for galaxies with Hα star-formation rates $> 1h^{-2}$ $M_\odot$ yr^{-1}.

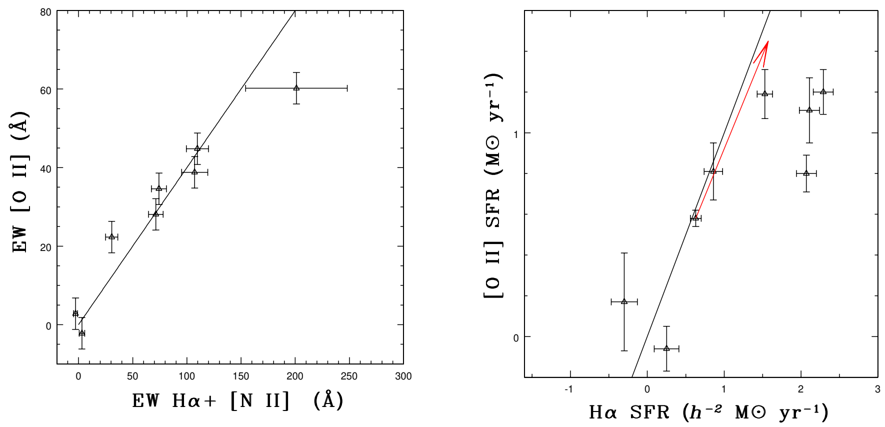

Fig. 1.3. Comparison between [O II] and Hα-derived equivalent widths (left) and star-formation rates (right) for eight cluster members. Red arrow in right panel shows redenning vector for 1 magnitude of extinction at Hα.

1.4 Summary

We present Hα-derived star-formation rates for the galaxy cluster CL J0023+0423B (z = 0.845) and demonstrate that near-infrared narrow-band imaging is a powerful way to sample the entire star-forming and post-starburst galaxy population in distant clusters. Comparison with spectroscopy shows that the number of false detections is low, and our Hα equivalent widths show reasonable correlation with spectroscopically determined [O II] equivalent widths. CL J0023+0423B is an excellent target for our narrow-band imaging study because of the wealth of published photometry, spectroscopy, and morphologies that we can correlate with our narrow-band imaging. Also, the low mass implied from low velocity dispersion, the lack of X-ray emission, and the predominantly spiral morphologies gave us good reason to expect significant Hα detections. However, for these same reasons, CL J0023+0423B does not allow for straightforward comparison to other intermediate redshift clusters which are X-ray selected. Results on the entire sample of seven $z \approx 0.8$ clusters will be published in the near future, and we will be able to form a more comprehensive picture of the star-formation properties of $z \approx 0.8$ galaxy clusters.

References

Balogh, M. L., Morris, S. L., Yee, H. K. C., Carlberg, R. G., & Ellingson, E. 1997, ApJL, 488, L75+
Balogh, M. L., Schade, D., Morris, S. L., Yee, H. K. C., Carlberg, R. G., & Ellingson, E. 1998, ApJL, 504, L75+
Bertin, E., & Arnouts, S. 1996, A&AS, 117, 393
Butcher, H., & Oemler, A. 1984, ApJ, 285, 426
Kennicutt, R. C. 1992a, ApJS, 79, 255
—. 1992b, ApJ, 388, 310
—. 1998, ARA&A, 36, 189
Lubin, L. M., Postman, M., Oke, J. B., Ratnatunga, K. U., Gunn, J. E., Hoessel, J. G., & Schneider, D. P. 1998, AJ, 116, 584

McCarthy, D. W., Ge, J., Hinz, J. L., Finn, R. A., & de Jong, R. S. 2001, PASP, 113, 353
Peng, C. Y., Ho, L. C., Impey, C. D., & Rix, H. 2002, AJ, 124, 266
Postman, M., Lubin, L. M., & Oke, J. B. 1998, AJ, 116, 560
—. 2001, AJ, 122, 1125
Zaritsky, D., Nelson, A. E., Dalcanton, J. J., & Gonzalez, A. H. 1997, ApJL, 480, L91+